Inorganic Chemistry

pubs.acs.org/IC
Article

Ionothermal Synthesis of Selenido Metalates in Tunable Aryl Alkyl Ionic Liquids (TAAILs)

Gina Stuhrmann, Zhou Wu, Isabell Nußbruch, Swantje Lerch, Bastian Weinert, Lukas Guggolz, Thomas Strassner,* and Stefanie Dehnen*

Cite This: https://doi.org/10.1021/acs.inorgchem.5c05009
Read Online

ABSTRACT: We report on the first reactions of selenido germanates in tunable aryl alkyl ionic liquids (TAAILs), namely, the treatment of $[K_4(H_2O)_3][Ge_4Se_{10}]$ with $SnCl_4 \cdot 5H_2O$ in $(Ph_{4\text{-}Br}C_6Im)[NTf_2]$, $(Ph_{4\text{-}Br}C_8Im)[NTf_2]$, $(Ph_{4\text{-}Br}C_{12}Im)[NTf_2]$, $(Ph_{2\text{-}Me}C_8Im)[NTf_2]$, and $(Ph_{4\text{-}OMe}C_8Im)(NTf_2)$, in the presence of 2,6-dimethylmorpholine (DMMP) as a basic auxiliary agent ($Ph_{Y\text{-}X}$ denotes a Ph group in the 1-position of the imidazolium cation (Im); the numeral Y specifies the *ortho* (2) or *para* (4) position of a substituent X at the Ph ring; and C_n denotes a linear alkyl substituent with *n* C atoms in the 3-position of the Im ring; NTf_2 = bis(trifluoromethan)sulfonimide). The use of different TAAILs allowed the observation of different products: $(Cat)_{24}[Ge_{24}Sn_{36}Se_{132}]$ (**1**), $(Ph_{2\text{-}Me}C_8Im)_2(DMMPH)_2[Ge_{1.4}Sn_{4.6}Se_{14}]$ (**2**), $(Cat)_6[GeSn_8Se_{21}]$ (**3**), $(Cat)_2[Sn_3Se_7]$ (**4**), and $(DMMPH)_4[Ge_4Se_{10}]$ (**5**). The compounds comprise cations from the corresponding TAAIL or $(DMMPH)^+$, which is the monoprotonated derivative of DMMP that forms *in situ* (note that in some cases, extreme disorder of the cations did not allow their localization on the difference *Fourier* map; these are referred to as 'Cat' in their formula). We discuss the anionic substructures in comparison to those of known compounds based on Ge, Sn, and Se atoms and report the effect of the different architectures on optical absorption properties.

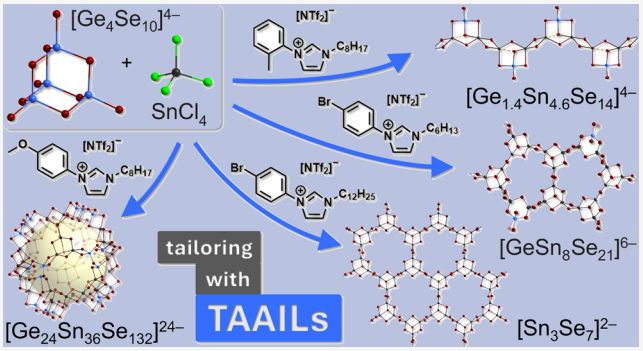

1. INTRODUCTION

Syntheses of chalcogenido metalate compounds have been the subject of multifaceted research endeavors over the last few decades. Chalcogenido metalate compounds exhibit exciting chemical and physical properties: fast ion conductivity,[1−4] photocatalytic activity,[5−9] and ion-exchange capability,[10−14] which could lead to potential applications in several areas, such as energy storage.[15−19]

Ionic liquids with their unusual properties, e.g., negligible vapor pressure and high thermal stability, can be used as alternatives to conventional solvents. They are useful reaction media due to their high variability, e.g., regarding cation/anion composition or pH value.[20−22] As compared to reactions in classical solvents as reaction media, chalcogenido metalate compounds prepared in ionic liquids oftentimes possess different compositions that can come along with very unusual structural motifs of their underlying anionic substructures.[23−28] The tunability of ionic liquids, through the virtually unlimited choice of cations and anions, allows for a precise control of the reaction conditions and, consequently, the synthesis of previously inaccessible compounds. One means of defining the properties of the respective reaction medium is the appropriate choice of the cation, which can also serve as a structural template for the anionic substructures.[29,30] Most frequently, imidazolium-based ionic liquids of the type $(C_lC_mC_nIm)[An]$ have been used in corresponding reactions (l, m, n: number of carbon atoms in the linear alkyl chains attached to the Im ring positions 1, 2, 3, respectively; $[An]^-$: $[BF_4]^-$ or a halide ion).[31,32]

Recently, the selective partial methylation of chalcogenido metalate anions was achieved by transfer of methyl groups from such ionic liquid cations onto the terminal chalcogenide ligands of the clusters.[33] It turned out that a selective methyl transfer takes place if at least one of the two alkyl substituents attached to the N atoms of the imidazolium cation is a methyl group. A selectively butylated supertetrahedral sulfido-oxo stannate cluster anion could eventually be accessed by using a doubly butylated ionic liquid, hence not displaying any methyl substituent at all. Salts of this cluster are soluble in common solvents (e.g., CH_3CN) due to the reduced overall charge and the lower polarity owing to the presence of butyl groups.

Received: October 25, 2025
Revised: November 5, 2025
Accepted: November 12, 2025

Notably, the small number of organic groups leaves the optical absorption energy nearly unaffected, as confirmed by experimental studies as well as time-dependent density functional theory (TD-DFT) calculations. This is in clear contrast to the notable widening of the optical band gap of metal chalcogenide clusters that are fully shielded by organic groups.[31] The findings were subsequently expanded to corresponding clusters bearing propyl, pentyl, or hexyl groups at the terminal S atoms.[34] Imidazolium-based ionic liquids can also be used for the controlled and limited aggregation of the anionic molecules into oligomers, thereby again reducing the negative charge per cluster unit and thus allowing for better solubility in common solvents like DMF.[35]

Tunable aryl alkyl ionic liquids (TAAILs)[36−40] differ from the mentioned imidazolium-based ionic liquids by replacement of the alkyl substituent at the N-site in the 1-position of the imidazolium ring with a phenyl ring, which in addition carries a substituent in *para*- or *ortho*-position. This substituent enables additional fine-tuning of the chemical and physical properties of the ionic liquid's cation, which is the basis for the denomination as 'TAAILs'.[41] Their physicochemical properties have been evaluated concerning thermal properties, viscosities, and electrochemistry.[38] By using DFT calculations, it could be shown that the distribution of the electron density between standard ionic liquids and TAAILs is significantly different. For the previously known alkyl-alkyl systems like 1,3-dimethylimidazolium (C_1C_1Im) or 1,3-butylmethylimidazolium (C_4C_1Im), the positive charge is mostly located on the alkyl groups, while TAAILs carry most of the charge (≈ 70%) at the imidazolium core.[41] To date, TAAILs have been used in transition-metal catalysis,[42] metal extraction,[43] and metal nanoparticle synthesis.[44−46]

We were interested in exploring the effect of using TAAILs on the product spectrum during the formation of chalcogenido metalate compounds. We studied the reactions with regard to the following aspects: (a) transformations of chalcogenido germanates and synthesis of chalcogenido metalates and (b) a variety of (new) structural motifs. Herein, we present our findings and discuss and compare them with respect to previous studies on common ionic liquids.

2. EXPERIMENTAL SECTION

2.1. General. All reactions (except the syntheses of the ionic liquids) and measurements were carried out in a dry argon atmosphere under strong exclusion of oxygen and moisture using standard Schlenk techniques or a glovebox (type Unilab plus; MBraun). The starting material $[K_4(H_2O)_3][Ge_4Se_{10}]$ was prepared in a way similar to a synthesis protocol described in the literature,[47,48] by reacting stoichiometric amounts of K_2Se, Ge, and Se (1:2:4) in an evacuated quartz ampule. The mixture was heated to 850 °C and maintained at this temperature for 32 h before allowing the mixture to cool down to room temperature. The obtained yellow powder was stirred in 50 mL of degassed water at 45 °C for 30 min, dried under vacuum, and stored under an argon atmosphere. K_2Se was synthesized by reacting stoichiometric amounts of K and Se in liquid ammonia according to the literature.[49] Ge (powder, Sigma-Aldrich, 99.999%), Se (powder, Sigma-Aldrich > 99.5%), and K lumps (Acros Organics, 98%) were used as received. $(Ph_{4\text{-}Br}C_6Im)[NTf_2]$ (1-(4-bromphenyl)-3-hexyl-1H-imidazolium bis(trifluoromethan)sulfonimide), $(Ph_{4\text{-}Br}C_{12}Im)[NTf_2]$ (1-(4-bromphenyl)-3-dodecyl-1H-imidazolium bis(trifluoromethan)sulfonimide), $(Ph_{4\text{-}OMe}C_8Im)[NTf_2]$ (1-(4-methoxyphenyl)-3-octyl-1H-imidazolium bis(trifluoromethan)-sulfonimide), and $(Ph_{2\text{-}Me}C_8Im)[NTf_2]$ (1-(2-methylphenyl)-3-octyl-1H-imidazolium-bis(trifluoromethan)sulfonimide) were prepared according to a literature method.[38] 2,6-Dimethylmorpholine (DMMP, Sigma-Aldrich, 99.8%) was distilled and stored over a molecular sieve (3 Å). For a list of used chemicals, see Table S1.

The synthetic procedure was the same for compounds **1**−**5**. 56 mg (0.043 mmol) of $[K_4(H_2O)_3][Ge_4Se_{10}]$ and 60 mg (0.17 mmol) of $SnCl_4{\cdot}5H_2O$ were weighed into a borosilicate glass ampule with a volumetric capacity of 7 mL. Tunable aryl alkyl ionic liquids and auxiliary were added. The ampule was sealed under vacuum. The ampule was then heated in an oven (Nabertherm) to 150 °C at a heating rate of 30 °C/h, kept at 150 °C for 72 h, and then cooled down to room temperature at a cooling rate of 5 °C/h. Details of the composition of the reaction mixtures are given below. "Cat" indicates the presence of cations that could not be determined in full from the difference *Fourier* map. The crystals were manually selected under a microscope after unit-cell determination, washed with acetonitrile, dried in dynamic vacuum, and subsequently weighed. The yield was calculated based on the initial amount of $SnCl_4{\cdot}5H_2O$ used for the reaction. Besides the formation of compounds **1**−**5**, SnSe, GeSe, and elemental Sn were identified as byproducts. It should be noted that the cation $(DMMPH)^+$, which represents the monoprotonated derivative of DMMP, forms *in situ*.

2.1.1. Synthesis of $(Cat)_{24}[Ge_{24}Sn_{36}Se_{132}]$ (**1**). 500 mg of $(Ph_{4\text{-}OMe}C_8Im)[NTf_2]$ and 37 μL of DMMP were added. After cooling, **1** was obtained in the form of red block-like crystals in approximately 62% yield.

2.1.2. Synthesis of $(Ph_{2\text{-}Me}C_8Im)_2(DMMPH)_2[Ge_{1.4}Sn_{4.6}Se_{14}]$ (**2**). 500 mg of $(Ph_{2\text{-}Me}C_8Im)[NTf_2]$ and 100 μL of DMMP were added. After cooling, **2** was obtained in the form of orange, plate-shaped crystals in approximately 47% yield.

2.1.3. Synthesis of $(Cat)_6[GeSn_8Se_{21}]$ (**3**). 500 mg of $(Ph_{4\text{-}Br}C_6Im)$-$[NTf_2]$ and 100 μL of DMMP were added. After cooling, **3** was obtained in the form of orange needles in approximately 26% yield.

2.1.4. Synthesis of $(Cat)_2[Sn_3Se_7]$ (**4**). 500 mg of $(Ph_{4\text{-}Br}C_{12}Im)$-$[NTf_2]$ and 100 μL of DMMP were added. After cooling, **4** was obtained in the form of orange, block-shaped crystals in approximately 76% yield.

2.1.5. Synthesis of $(DMMPH)_4[Ge_4Se_{10}]$ (**5**). 500 mg of $(Ph_{4\text{-}Br}C_8Im)[NTf_2]$ and 100 μL of DMMP were added. After cooling, **5** was obtained in the form of orange, block-shaped crystals in approximately 81% yield.

2.1.6. Single-Crystal X-ray Diffraction. Crystals suitable for X-ray diffraction analyses of compounds **1** and **4** were investigated with Ga−Kα radiation (λ = 1.34143 Å) at T = 180 K on the area detector system STOE StadiVari. Compounds **2** and **5** were investigated with a Bruker D8 Quest with a microfocus source emitting Mo−Kα radiation (λ = 0.71073) and a Photon 100 detector at T = 100 K. Compound **3** was investigated with a STOE StadiVari diffractometer at 100 K, using Cu−Kα radiation (λ = 1.54186) from an X-ray micro source with X-ray optics and a Pilatus 300 K Si hybrid pixel array detector. Structure solution by dual space methods and full-matrix least-squares refinement against F^2 were carried out using SHELXT15, SHELXL15, and OLEX2 software.[37] All nonhydrogen atoms were refined using anisotropic displacement parameters. H atoms were calculated by using a riding model. Crystallographic data for the structures reported in this paper have been deposited with the Cambridge Crystallographic Data Centre as supplementary publication no. CCDC-2483737 (**2**), CCDC-2483738 (**3**), CCDC-2483739 (**4**), and CCDC-2483740 (**5**).

2.1.7. UV−Visible Spectroscopy. The optical absorption properties of compounds **1**−**5** and of $[K_4(H_2O)_3][Ge_4Se_{10}]$ were measured under inert conditions employing a Varian Cary 5000 UV/vis/NIR spectrometer from Agilent, equipped with a Praying Mantis accessory for solid-state samples. To determine the optical band gaps, the raw data were transformed from reflectance R to absorption according to the Kubelka-Munk function:[34,35]

$$F(R) = \frac{k}{s} = \frac{(1 - R_\infty)^2}{2R_\infty}$$

https://doi.org/10.1021/acs.inorgchem.5c05009
Inorg. Chem. XXXX, XXX, XXX−XXX

Scheme 1. Illustration of the Anions of the Different Reaction Products Emerging from Reactions of $[K_4(H_2O)_3][Ge_4Se_{10}]$ and $SnCl_4 \cdot 5H_2O$ in the Presence of 2,6-Dimethylmorpholine (DMMP) in TAAILs (1−4; Top, Black Lines), or in the Common Ionic Liquid $(C_4C_1Im)[BF_4]$ (I and II; Bottom; Gray Lines), under Otherwise Same Conditions; the Anionic Structure of Compound 5 Is Not Drawn, as It Is the Same as That of the Precursor[a]

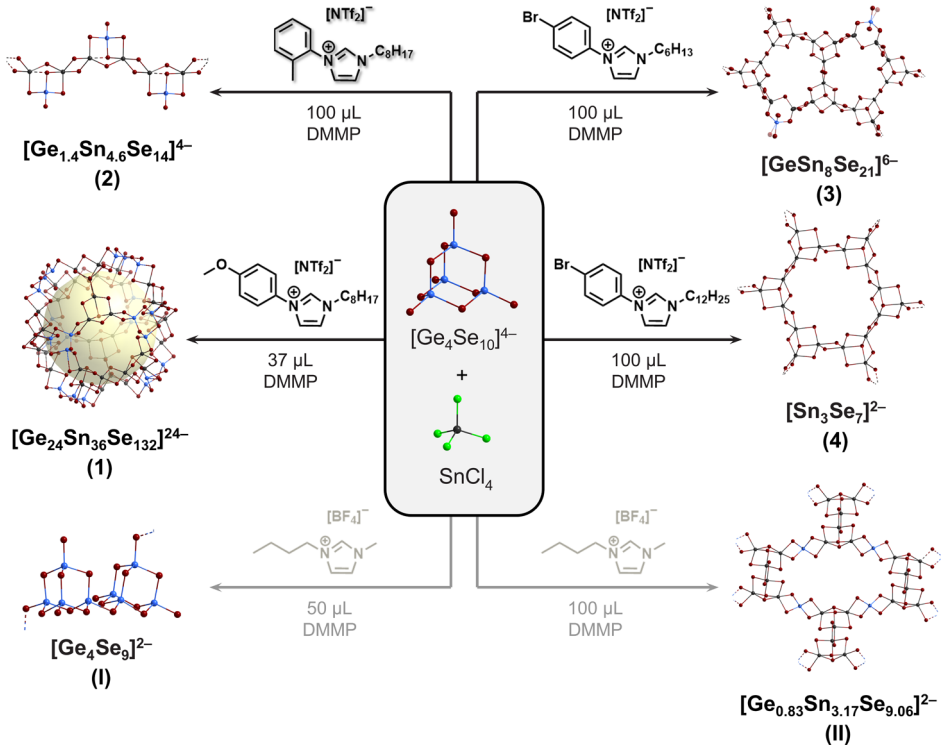

[a]All atoms are drawn in ball-and-stick mode, Se: red, Sn: dark gray, Ge: light blue. Only anionic substructures are illustrated, counter ions are omitted for clarity.

Table 1. Selected Structural Parameters of Compounds 2−5[a]

parameter	2	3	4	5
Ge-(μ_3-Se)	2.3774(12)−2.3793(13)			
Sn-(μ_3-Se)	2.953(11)−2.9770(11)	2.8413(23)	2.7586(7)	
(Sn/)Ge-(μ-Se)$_{in}$	2.4058(11)−2.4254(11)	2.4466(22)		2.3771(9)− 2.3963(12)
Sn-(μ-Se)$_{in}$	2.5136(12)−2.5272(10)	2.5114(18)−2.5592(19)	2.5583(9)	
(Sn/)Ge−Se$_{ex}$	2.3076(13)−2.3134(13)	2.3241(37)−2.3687(35)		2.2796 (16)
Sn-(μ-Se)$_{ex}$	2.4938(10)−2.6460(11)	2.4818(25)−2.7734(21)	2.5175(9)− 2.6872(9)	
Se−Sn−Se	95.044(36)−124.020(39)	87.422(60)−124.579(64)	87.525(21)− 122.083(26)	
Sn−Se−Sn	87.087(33)−101.619(35)	85.008(60)−95.710(64)	86.046− 94.735(25)	
(Sn/)Ge−Se−Sn	89.542(38)−93.449(39)	92.886(79)		
Se−Ge−Se	103.924(43)−119.711(49)	102.037(90)− 120.391(89)		108.935(7)− 112.080(5)
Ge−Se−Ge				105.889(6) 106.300(2)

[a]Distances are given in Å, and angles are given in °. Indices refer to internal ("in") bonds within the $\{T_4Se_3\}$ defect-heterocubane units (T = Ge, Sn) or to external ("ex") bonds to μ-bridging Se atoms between the different subunits, respectively.

where k is the K-M absorption coefficient, R_∞ is the diffuse reflection, and s is the K-M scattering coefficient.[50,51] Tauc plots were generated by plotting

$$(F(R_\infty) \times h\nu)^{1/\gamma}$$

as a function of the photon energy $h\nu$. The power coefficient can be $\gamma = 1/2$, $2/3$, 2, or 3, depending on the nature of the transition, which corresponds to direct allowed, direct forbidden, indirect allowed, or indirect forbidden transitions, respectively. E_g is estimated from the intercept with the x axis of the linear fit from the corresponding region. Since the transition in the region of interest was far more pronounced when choosing $\gamma = 2$, we assume that all analyzed compounds feature an indirect band gap.[50−54]

2.1.8. Fourier-Transform Infrared Spectroscopy. *Fourier*-transform infrared (FTIR) spectra were recorded on a Nicolet Summit X FTIR Spectrometer (ThermoFisher Scientific) in the wavenumber range 4000−400 cm^{-1}. The instrument is located inside a glovebox, to enable measurements of air- and moisture-sensitive solid samples.

3. RESULTS AND DISCUSSION

In Scheme 1 (top), we give an overview of the products of reactions of $[K_4(H_2O)_3][Ge_4Se_{10}]$ with $SnCl_4 \cdot 5H_2O$ in the presence of DMMP in TAAILs, which were obtained as single crystals (Figure S6). As mentioned in Section 2, cations are indicated explicitly in the sum formulas, if they could be localized on the difference *Fourier* map and could hence be

https://doi.org/10.1021/acs.inorgchem.5c05009
Inorg. Chem. XXXX, XXX, XXX−XXX

identified, or as "Cat" in cases where disorder prohibited their localization. It should be noted that this is a rather typical finding in such systems. The new compounds are given as $(Cat)_{24}[Ge_{24}Sn_{36}Se_{132}]$ (**1**), $(Ph_{2-Me}C_8Im)_2(DMMPH)_2[Ge_{1.4}Sn_{4.6}Se_{14}]$ (**2**), $(Cat)_6[GeSn_8Se_{21}]$ (**3**), $(Cat)_2[Sn_3Se_7]$ (**4**), and $(DMMPH)_4[Ge_4Se_{10}]$ (**5**). For comparison, products of corresponding reactions undertaken in the common ionic liquid $(C_4C_1Im)[BF_4]$ under otherwise similar reaction conditions are also shown in Scheme 1 (bottom). Although some of the anionic frameworks have also been accessible in common ionic liquids, like the salts comprising the 'zeoball' anion $[Ge_{24}Sn_{36}Se_{132}]^{24-}$[24−27] or the 2D-$\{[Sn_3Se_7]^{2-}\}$ substructure (middle row),[55] the overview in Scheme 1 indicates that the reaction medium mostly has a notable impact on the product spectrum.

The compositions of compounds **1**−**5** were confirmed by micro-X-ray fluorescence spectroscopy (μ-XFS) analysis (see Figures S7−S10 and Tables S2−S5). Their structures were determined by means of single-crystal X-ray diffraction and are described below. Selected structural parameters are summarized in Table 1. More details of the X-ray diffraction analyses are provided in Tables S6−S10, Figures S11 and S12. We further demonstrate the effect of the anionic architecture on the optical absorption properties.

The reaction in $(Ph_{4\text{-}OMe}C_8Im)[NTf_2]$ in the presence of 100 μL DMMP affords single crystals of compound **1** in yields of 42−63%, depending on details of the procedure (detailed information regarding all synthetic procedures is given in the Supporting Information). The compound crystallizes in the monoclinic crystal system, space group *C*2/*m*, with two formula units per unit cell. It represents a new salt of the 'zeoball' anion $[Ge_{24}Sn_{36}Se_{132}]^{24-}$.[27] Owing to the limited scattering power of the crystals, the number of single-crystal data did not allow for a refinement of the many parameters of this structure, but the data were sufficient to unambiguously identify the very prominent anion, which we present here as a structural model; an explanation of the situation and basic crystallographic data including the unit cell parameters are provided in Table S6. It consists of two subunits, $\{Ge_3Se_9\}$ and $\{Sn_6Se_{18}\}$, which are connected via μ-Se atoms (Scheme 2).

Scheme 2. Subunits of the $[Ge_{24}Sn_{36}Se_{132}]^{24-}$ Anion[a]

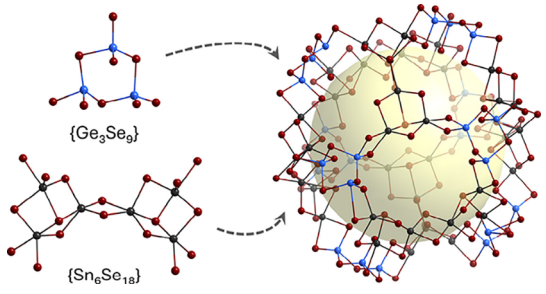

[a]The inner cavity has a diameter of 15.4 Å by the smallest center-to-center distance of opposite Se atoms and 11.6 Å (illustrated as a sphere) upon consideration of van der Waals radii.

Owing to heavy disorder, which contributes to the limited data quality, the $(Ph_{4\text{-}OMe}C_8Im)^+$ cations of **1** could only be partially localized on the difference *Fourier* map. As found for other salts of the $[Ge_{24}Sn_{36}Se_{132}]^{24-}$ anion,[24,27,56] they are situated in the voids between the anions and can also—partially or fully—occupy the inner cavity of the anionic spheres.

Employing a TAAIL with a methyl group in the *ortho*-position of the Ph ring instead of a methanolate substituent in *para*-position affords single crystals of compound **2** in approximately 47% yield. The compound crystallizes in the monoclinic crystal system, space group type $P2_1/n$, with four formula units per unit cell. The anionic structure consists of $\{Ge_{0.7}Sn_{2.3}Se_7\}^{2-}$ defect-heterocubane-type building units that are connected by μ-Se bridges to form alternating one-dimensional strands along ⟨010⟩. However, the $\{Ge_{0.7}Sn_{2.3}Se_7\}^{2-}$ units exhibit a mixed occupancy of Ge and Sn atoms on one of the group 14 atom positions, as confirmed both through the refinement of the single-crystal X-ray diffraction data and μ-XFS analysis (percentages found for Ge, Sn, Se = 7.62%, 23.13%, 69.24%, see Table S3). This is reflected by differences in bond lengths and angles: definite Sn−Se bond lengths range from 2.4938(10) to 2.9533(11) Å, while the Sn/Ge−Se bond lengths are shorter on average, 2.3076(14)−2.4246(11) Å. The definite Se−Sn−Se angles within one building unit exhibit values from 114.394(38) to 116.439(39)°; values including the μ-Se atoms between the building units are 95.044(36)−124.020(39)°. The Se−Sn/Ge−Se angles range from 103.924(43) to 119.711(49)°. The Sn−Se−Sn angle within the defect-heterocubane cages is 101.619 (35)°, and the Sn/Ge−Se−Sn angles amount to 89.542(38) and 93.449(39)°. Sn−Se−Sn angles including the μ-Se bridges between the building units range from 87.087(33) to 87.817(34)° (Table 1).

The negative charge is compensated by two ionic liquid cations and two protonated DMMP molecules per formula unit of compound **2**. Half of the channels that extend between the anionic strands in the ⟨010⟩ direction are filled with $(DMMPH)^+$ cations, and the other half is filled with $(Ph_{4\text{-}Me}C_8Im)^+$ cations. Notably, the two types of cations remain separate in their respective channels.

The closest Se···Se distance between atoms from two adjacent strands in the *c* direction is 5.2525(13) Å, while the closest Se···Se distances in the *a* direction range from 6.4566(14) to 7.0775(14) Å. As expected, the smaller cation $(DMMPH)^+$ fills the voids between the strands. Figure 1 illustrates the crystal structure of compound **2**.

The use of $(Ph_{4\text{-}Br}C_6Im)[NTf_2]$, in which the substituent in *para*-position is a Br atom and the alkyl part is a hexyl group, results in the formation of yellow crystals of compound **3** in approximately 26% yield. **3** crystallizes in the monoclinic crystal system, space group type $P2_1/m$, with four formula units per unit cell. The anionic structure consists of $\{Sn_3Se_7\}^{2-}$ and $\{GeSn_2Se_7\}^{2-}$ defect-heterocubane-type building units in a 2:1 ratio that are connected *via* μ-Se atoms into five-membered macrocycles. The latter are fused *via* sharing of two connected $\{Sn_3Se_7\}^{2-}$ units each into a one-dimensional strand running along ⟨010⟩. Sn−Se bond lengths range from 2.4818(25) to 2.8413(23) Å, while the Ge−Se bond lengths are naturally slightly shorter, 2.3241(37)−2.4466(22) Å (Table 1). All bond lengths are in good agreement with reported values.[57−60] The Se−Sn−Se angles within one building unit range from 87.422(60) to 119.287(63)°, while the values including the μ-bridging Se atoms are in the range from 87.422(60) to 125.494(79)°. The Se−Ge−Se angles exhibit values from 102.037(90) to 120.391(89)°.

The Sn−Se−Sn angles within the defect-heterocubane cages range from 85.008 (60) to 95.710 (64)°, the Sn−Se−Sn angles including the μ-Se bridges range from 85.904(67) to

https://doi.org/10.1021/acs.inorgchem.5c05009
Inorg. Chem. XXXX, XXX, XXX−XXX

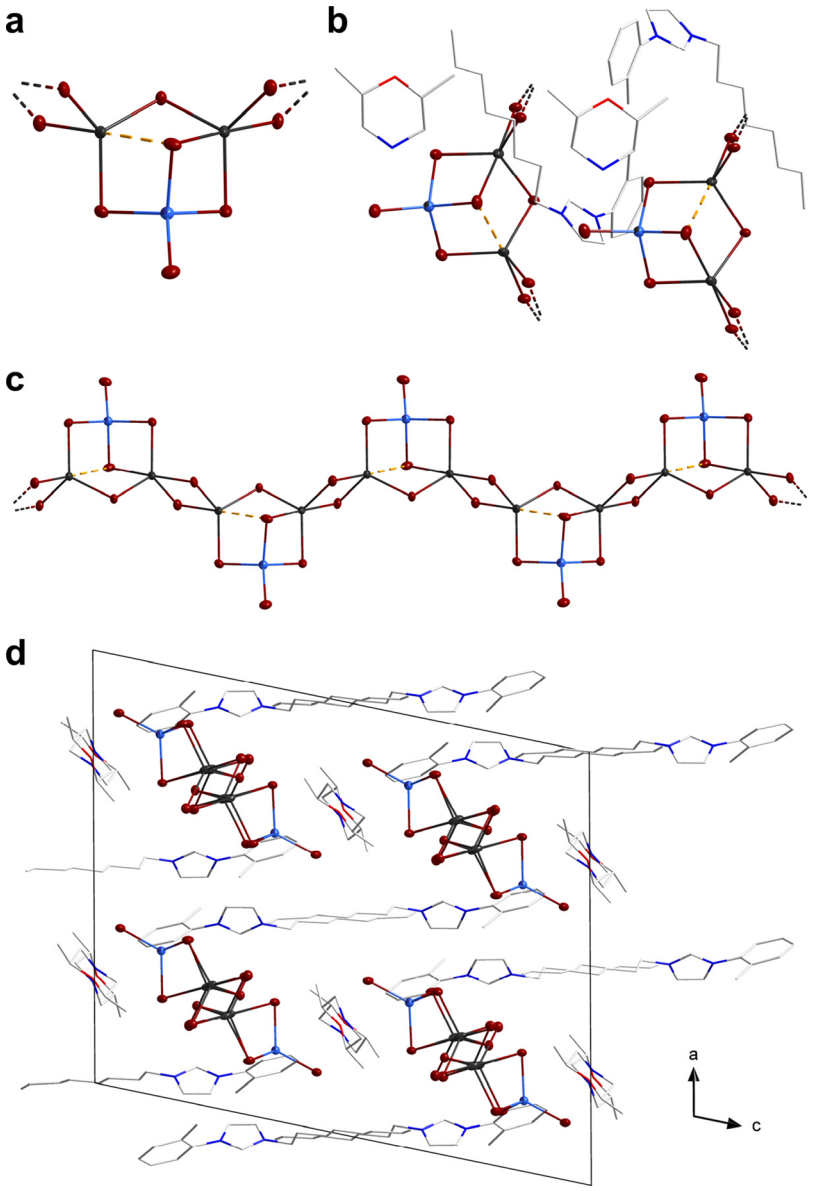

Figure 1. Crystal structure of **2**. (a) Ternary building unit of the anion in **2**. (b) Asymmetric unit including cations. (c) View of the section of one anionic strand. (d) Packing of cations and anions in the crystal, viewed along the crystallographic *b* axis. Thermal ellipsoids of Ge, Sn, and Se atoms are drawn at the 50% probability level. Cations are shown in wire representation. Se: red, Sn: dark gray, Ge/Sn: light blue, C: gray, N: blue, and O: red. H atoms have been omitted for the sake of clarity.

88.971(71)°, and the Ge−Se−Sn angle is 92.886(79)° (Table 1).

The cations could not be localized on the difference *Fourier* map, which is a very typical finding for reactions under solvothermal or ionothermal conditions. However, the cations are assumed to be $(DMMPH)^+$ molecules according to the number of electrons (720 e^- in a volume of 3979Å^{-3} in one void per unit cell) found in the voids between the anions, which accords with the presence of three $(DMMPH)^+$ molecules per asymmetric unit or six per unit cell. The Se···Se distances between two layers range from 5.1125(27) to 5.7264(44) Å. Figure 2 illustrates the crystal structure of compound **3**.

The anionic substructures of compounds **2** and **3** are rare examples of a ternary Ge/Sn/Se architecture. Notably, all ternary anions with Ge/Sn/Se architecture reported so far were obtained from ionothermal syntheses. Besides various salts of the ternary 'zeoball' anion,[24,27] only four further types of ternary Ge/Sn/Se anions have been known to date: $[Ge_{0.83}Sn_{3.17}Se_{9.06}]^{2-}$ (**II**),[61] $[Cs@Sn^{II}{}_4(Ge^{IV}{}_4Se_{10})_4]^{7-}$ (**III**),[62] and $[Sn^{II}(Ge^{IV}{}_4Se_{10})]^{2-}$ (**IV**[62] and **V**;[61] see Scheme 1 and Figure 3). For comparison, we briefly describe the architectures here: compound **II** is built of one $\{Sn_6Se_{10}\}$ subunit and two $\{GeSe_4\}$ tetrahedra to form two-dimensional corrugated layers (Scheme 1). Compound **III** is based on four $\{Ge_4Se_{10}\}$ subunits, which are connected *via* four Sn^{II} atoms to form a supertetrahedral $[Sn^{II}{}_4(Ge^{IV}{}_4Se_{10})_4]^{8-}$ cluster anion embedding an endohedral Cs^+ cation (Figure 3a). The anionic substructures of compounds **IV** and **V** are also built of $\{Ge_4Se_{10}\}$ subunits, but here, the subunits are linked by sharing μ-Se atoms with $\{Sn^{II}Se_3\}$ units into one-dimensional double strands; both architectures differ in the mode of linkage of the two subunits (Figure 3b,c). While each $\{Sn^{II}Se_3\}$ unit

https://doi.org/10.1021/acs.inorgchem.5c05009
Inorg. Chem. XXXX, XXX, XXX−XXX

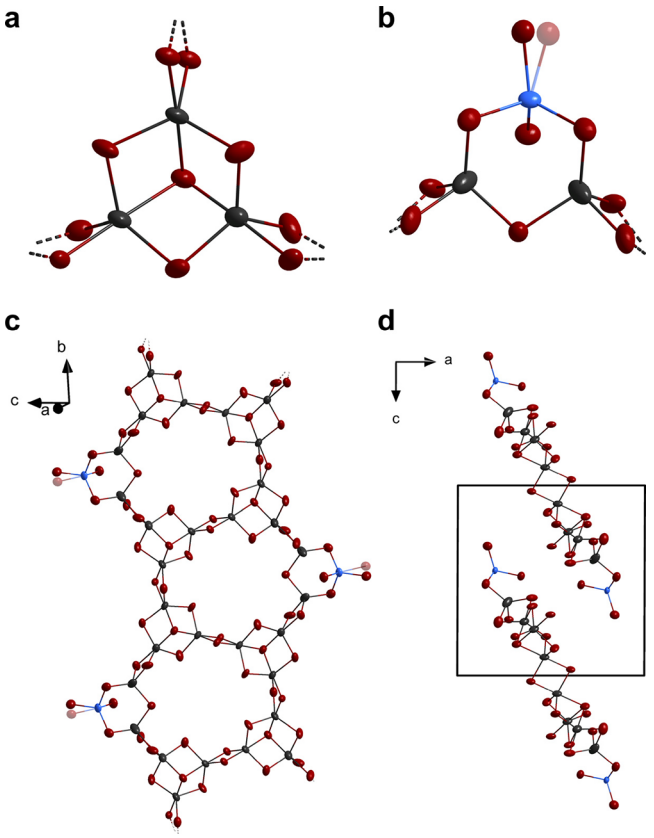

Figure 2. Crystal structure of **3**. (a) Binary building unit of the anion in **3**. (b) Ternary building unit of the anion in **3**. (c) Top view of the fused five-membered rings. (d) Packing of anions in the crystal, viewed along the crystallographic *b* axis. Thermal ellipsoids of Ge, Sn, and Se atoms are drawn at the 50% probability level. Se: red, Sn: dark gray, Ge: light blue. Disorder positions are shown in semitransparent mode.

bridges between two $\{Ge_4Se_{10}\}$ subunits in **IV**, the $\{Sn^{II}Se_3\}$ units in **V** connect three $\{Ge_4Se_{10}\}$ moieties each.

Compound **4** was obtained from treatment of the precursors in $(Ph_{4\text{-}Br}C_{12}Im)[NTf_2]$. The only change compared to the synthesis of compound **3** is the length of the alkyl group of the TAAIL, which in the synthesis of compound **4** is a dodecyl group. Compound **4** crystallizes as orange crystals in approximately 76% yield in the trigonal crystal system, space group $P\bar{3}$, with two formula units per unit cell. The motif of the anion in **4** is already known from other salts.[63−66] Notably, the $[K_4(H_2O)_3][Ge_4Se_{10}]$ starting material served only as a source of Se^{2-} to form the binary selenido stannate network in the reaction with $SnCl_4{\cdot}5H_2O$. As a consequence, exclusively $\{Sn_3Se_7\}^{2-}$ defect-heterocubane-type building units are connected in **4** *via* μ-Se atoms. The resulting pattern is a honeycomb-type $^2_\infty\{[Sn_3Se_7]^{2-}\}$ network of six-membered macrocycles that are annealed in the *ab* plane. The Se···Se distances between two honeycomb networks range from 6.0212(10) to 7.3947(13) Å.

The Sn−Se bond lengths within the anionic architecture range from 2.5175(9) to 2.7586(7) Å. These values are again in good agreement with reported lengths.[57−60] The Se−Sn−Se angles within one building unit show values from 87.525(21) to 115.674(25)°, while the values including the μ-bridging Se atoms are in the range 91.028(21)−122.083(26)°. The Sn−Se−Sn angles within the defect-heterocubane cages range from 86.046(12) to 94.735(25)°, and the Sn−Se−Sn angle including the μ-Se bridges is 89.713(26)° (Table 1).

While the imidazolium skeletons of the cations were localized on the difference *Fourier* map, the substituents were not localizable owing to inherent disorder. However, the imidazole rings clearly indicate that they are $(Ph_{4\text{-}Br}C_{12}Im)^+$ molecules. All of the cations are situated in the voids between the anions and arranged in layers. Compared to compound **3**, the distance between two layers increased with the longer alkyl chain—evidencing the TAAIL cations' roles as templating agents in these reactions. Figure 4 illustrates the structural features of compound **4**.

A different situation was reported regarding the role of imidazolium-based ionic liquids comprising alkyl chains of different lengths in the case of tellurido mercurates. In the compounds $(C_{10}C_1Im)_4[Hg_4Te_{12}]$, $(C_{10}C_1Im)_6[Hg_6Te_{10}(TeDec)_2]$ (Dec = decyl), $(C_{10}C_1Im)_6[Hg_6Te_{10}(TeDec)(TeMe)]$ (Me = methyl),[67] $(C_8C_1Im)_8[Hg_8Te_{16}]$, or $(C_{10}C_1Im)_8[Hg_8Te_{16}]$,[68] the alkyl chains assembled in a way that led to a lamellar arrangement of the tellurido mercurate anions in the crystal structures. Here, the tellurido mercurate units are always surrounded by the imidazolium rings of the cations, with the long alkyl chains directing outward and undergoing van der Waals interactions with other alkyl chains of neighboring cations.[67,68]

The use of $(Ph_{4\text{-}Br}C_8Im)[NTf_2]$, in which the substituent in *para*-position is a Br atom and the alkyl chain is an octyl group, results in the formation of yellow crystals of compound **5**. It crystallizes in the tetragonal system in the space group type $I4_1/amd$. Compound **5** comprises $\{Ge_4Se_{10}\}^{4-}$ anions exhibiting a T2-type supertetrahedral structure, like the anion of the starting material (therefore not shown in Scheme 1). The charge of 4− is compensated for by four $(DMMPH)^+$ cations. Thus, the K^+ cations from the starting material are simply replaced with the organic cation $(DMMPH)^+$ that forms in situ

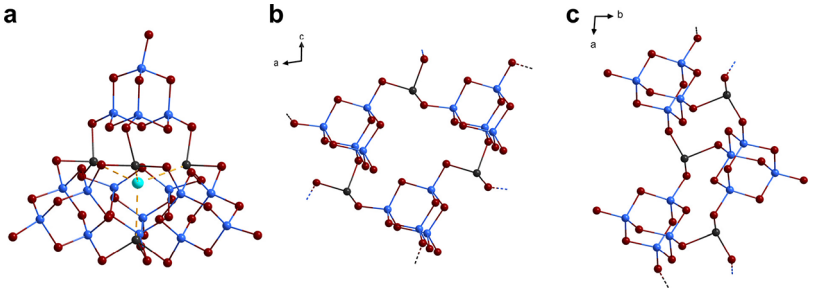

Figure 3. Examples of ternary anionic Ge/Sn/Se architectures. (a) $[Cs@Sn^{II}_4(Ge^{IV}_4Se_{10})_4]^{7-}$ in **III**.[46] (b) $[Sn^{II}(Ge^{IV}_4Se_{10})]^{2-}$ in **IV**. (c) $[Sn^{II}(Ge^{IV}_4Se_{10})]^{2-}$ in **V**. All atoms are drawn in ball-and-stick mode; Se: red, Sn: dark gray, Ge: light blue, Cs: turquoise.[61,62]

https://doi.org/10.1021/acs.inorgchem.5c05009
Inorg. Chem. XXXX, XXX, XXX−XXX

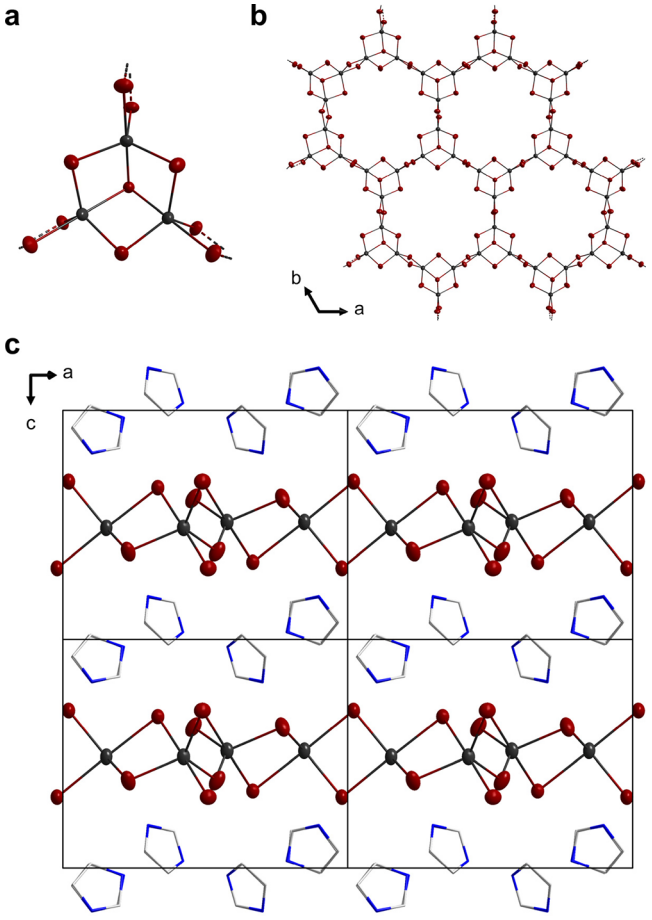

Figure 4. Crystal structure of **4**: (a) binary building unit of the anion in **4**. (b) Top view of a section of one of the honeycomb-type $^{2}_{\infty}\{[Sn_3Se_7]^{2-}\}$ layers. (c) 2 × 2 × 2 supercell of **4** viewed along the crystallographic *b* axis. Thermal ellipsoids of Sn and Se atoms are drawn at the 50% probability level. Fragments of the cations are shown in wire representation (disorder and H atoms omitted). Se: red, Sn: dark gray, C: gray, N: blue.

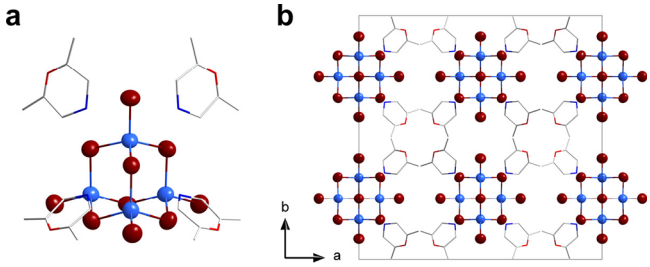

Figure 5. Crystal structure of **5**. (a) $[Ge_4Se_{10}]^{4-}$ anion with four closest $(DMMPH)^+$ cations. (b) Extended unit cell of **5** viewed along the crystallographic *c* axis. Thermal ellipsoids of Ge and Se atoms are drawn at the 50% probability level. Cations are shown in wire representation (H atoms omitted). Se: red, Ge: light blue, C: gray, N: blue, O: red.

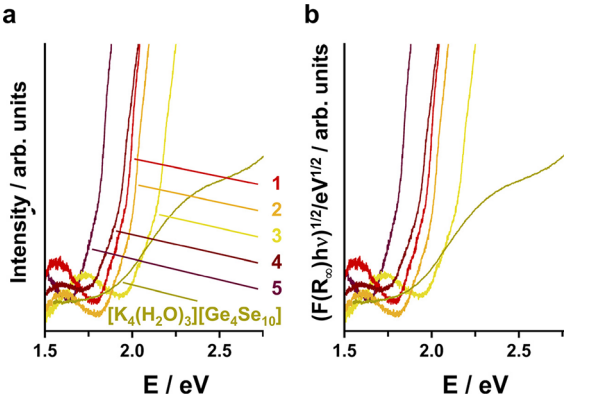

Figure 6. (a) UV-vis spectra of single crystals of $[K_4(H_2O)_3]$-$[Ge_4Se_{10}]$ and **1**−**5**. (b) Tauc plots generated by plotting $(F(R_\infty) \times h\nu)^{1/\gamma}$ as a function of the photon energy $h\nu$, with $\gamma = 2$ of $[K_4(H_2O)_3][Ge_4Se_{10}]$ and **1**−**5**. The color codes are the same in (a) and (b).

from the DMMP auxiliary and protons from crystal water in the starting compounds. The Ge−Se bond lengths in the anion range from 2.2796(16) to 2.3963(12) Å, with the external Ge−Se bonds (2.2796(16) Å) being shorter than the internal Ge−Se bonds (2.3771(9)−2.3963(12) Å), as typical and in agreement with reported values.[57] The Se−Ge−Se angles within one defect-heterocubane unit adopt values from 110.668(4)° to 112.080(5)°, while the angles including the external Se atoms are at 108.935(7)°. In the unit cell, every $[Ge_4Se_{10}]^{4-}$ cluster anion is surrounded by four $(DMMPH)^+$ cations such that the N atom always points in the direction of the cluster, thus allowing for optimal anion···cation charge compensation. Figure 5 illustrates the crystal structure of **5**.

3.1. Optical Properties. Although the compositions and underlying structural units of compounds $(Cat)_{24}[Ge_{24}Sn_{36}Se_{132}]$ (**1**), $(Ph_{2\text{-}Me}C_8Im)_2(DMMPH)_2[Ge_{1.4}Sn_{4.6}Se_{14}]$ (**2**), $(Cat)_6[GeSn_8Se_{21}]$ (**3**), $(Cat)_2[Sn_3Se_7]$ (**4**), and $(DMMPH)_4[Ge_4Se_{10}]$ (**5**) are not identical, their optical absorption properties and visible colors fall within a comparable range, suggesting that subtle variations in the structures can affect their electronic properties. UV-visible spectra were recorded to quantify the optical absorption properties (see Figures 6 and S13−S18). According to the Tauc plots, all compounds are indirect semiconductors, with band gaps between 1.76 and 2.25 eV. Changing the cation from K^+ to an organic cation like $(DMMPH)^+$ in salts of the binary $[Ge_4Se_{10}]^{4-}$ anion results in a minimal blue-shift of the absorption and a corresponding slight widening of the band gap (from 1.76 eV in $[K_4(H_2O)_3][Ge_4Se_{10}]$ to 1.80 eV in **5**).[69] Smaller molecular units $[Sn_3Se_7]^{2-}$, although being based on Sn/Se atoms and assembled into two-dimensional layers, also cause a slight blue-shift of the band gap in compound **4** (1.91 eV). The three ternary compounds show even larger band gaps—indicating the influence of admixing Ge to the compounds. However, the Ge:Sn ratio alone does not define the band gap, as this is a result of both the Ge:Sn:Se composition and the extension and dimensionality of the network. The nearly identical gaps in compound **1** (1.96 eV) and compound **2** (1.99 eV) indicate that the larger relative amount of Sn atoms in **2** is overcompensated by the overall larger amount of metal atoms in **1**. The composition of compound **3** is closely related to that of compound **4**; yet one out of nine Sn atoms is replaced with Ge. In addition, instead of a two-dimensional layer-type arrangement of six-membered macrocycles, the subunits assemble into five-membered macrocycles forming a one-dimensional strand. Hence, another widening of the gap to 2.13 eV seems understandable. Overall, the differences in optical absorption properties of the new compounds **1**−**5** are small, with all compounds forming yellow to orange crystals, in accordance with their optical absorption

https://doi.org/10.1021/acs.inorgchem.5c05009
Inorg. Chem. XXXX, XXX, XXX−XXX

properties. Obviously, the different characteristics of the anionic substructures regarding compositions, structural motifs, and dimensionalities, all of which affect the optical absorption properties, and the properties of the cations acting as separators between the anionic architectures seem to compensate each other in a way that allows for very similar electronic properties to result for the crystalline solids.

4. CONCLUSIONS

We reported the successful application of five different tunable aryl alkyl ionic liquids (TAAILs) for the ionothermal treatment of $[K_4(H_2O)_3][Ge_4Se_{10}]$ with $SnCl_4{\cdot}5H_2O$ and the synthesis of a series of new selenido metalate salts. Subtle changes of the nature of the TAAIL cations, that is, the substituent in the *ortho* or *para*-position of the Ph group attached to the N1-position of the imidazolium ring, led to different reaction products. We presented the crystal structures of the products that either represent salts of famous anions—the "zeoball" anion in **1**, the $^2_\infty\{[Sn_3Se_7]^{2-}\}$ honeycomb-type layer in **4**, or a new salt of the $[Ge_4Se_{10}]^{4-}$ anion—or comprise novel types of ternary anion types—one-dimensional strands of ternary Ge/Sn/Se defect-heterocubane-type building units in **2**, or alternating five-membered macrocycles built from two different defect-heterocubane-type building units in **3**. These findings illustrate that the dimensionality of the products can be tuned with the help of TAAIL cations. Although a direct correlation between the properties of a given cation and the structure of the product cannot be determined at this stage, the fact that some of the compounds were only accessible this way refers to the notable structure-directing effect of TAAILs. The optical absorption properties of the new compounds span a narrow range (1.76−2.13 eV), indicating a subtle compensation of effects based on the composition, structural motifs, and dimensionality of the chalcogenido metalate architecture, as well as the separation of anionic architectures by the cations.

■ ASSOCIATED CONTENT

Supporting Information

The Supporting Information is available free of charge at https://pubs.acs.org/doi/10.1021/acs.inorgchem.5c05009.

Syntheses, light microscopy, micro-X-ray fluorescence spectroscopy, X-ray diffraction, optical absorption spectroscopy, and FT-IR spectroscopy (PDF)

Accession Codes

Deposition Numbers 2483737−2483740 contain the supplementary crystallographic data for this paper. These data can be obtained free of charge *via* the joint Cambridge Crystallographic Data Centre (CCDC) and Fachinformationszentrum Karlsruhe Access Structures service.

■ AUTHOR INFORMATION

Corresponding Authors

Thomas Strassner − *Physikalische Organische Chemie, Technische Universität Dresden, 01069 Dresden, Germany*; Email: thomas.strassner@tu-dresden.de

Stefanie Dehnen − *Institute of Nanotechnology, Karlsruhe Institute of Technology, 76131 Karlsruhe, Germany*; orcid.org/0000-0002-1325-9228; Email: stefanie.dehnen@kit.edu

Authors

Gina Stuhrmann − *Institute of Nanotechnology, Karlsruhe Institute of Technology, 76131 Karlsruhe, Germany*; orcid.org/0009-0007-0660-2298

Zhou Wu − *Institute of Nanotechnology, Karlsruhe Institute of Technology, 76131 Karlsruhe, Germany*

Isabell Nußbruch − *Fachbereich Chemie und Wissenschaftliches Zentrum für Materialwissenschaften, Philipps-Universität Marburg, 35043 Marburg, Germany*

Swantje Lerch − *Physikalische Organische Chemie, Technische Universität Dresden, 01069 Dresden, Germany*

Bastian Weinert − *Institute of Nanotechnology, Karlsruhe Institute of Technology, 76131 Karlsruhe, Germany*

Lukas Guggolz − *Institute of Nanotechnology, Karlsruhe Institute of Technology, 76131 Karlsruhe, Germany*

Complete contact information is available at: https://pubs.acs.org/10.1021/acs.inorgchem.5c05009

Author Contributions

The manuscript was written through contributions of all authors. All authors have given approval to the final version of the manuscript.

Notes

The authors declare no competing financial interest.

■ ACKNOWLEDGMENTS

This work was supported by the German Research Foundation (Deutsche Forschungsgemeinschaft, DFG) in the framework of the Priority Programme SPP 1708. The authors thank Björn Koch for his help with μ-XFS measurements. G.S. acknowledges a fellowship from the German Academic Exchange Service (DAAD). The authors gratefully acknowledge the support by the Karlsruhe Nano Micro Facility (KNMFi).

■ REFERENCES

(1) Zheng, N.; Bu, X.; Feng, P. Synthetic Design of Crystalline Inorganic Chalcogenides Exhibiting Fast-Ion Conductivity. *Nature* **2003**, *426*, 428−432.

(2) Kamaya, N.; Homma, K.; Yamakawa, Y.; Hirayama, M.; Kanno, R.; Yonemura, M.; Kamiyama, T.; Kato, Y.; Hama, S.; Kawamoto, K.; Mitsui, A. A Lithium Superionic Conductor. *Nat. Mater.* **2011**, *10*, 682−686.

(3) Bron, P.; Johansson, S.; Zick, K.; Schmedt Auf Der Günne, J.; Dehnen, S.; Roling, B. $Li_{10}SnP_2S_{12}$: An Affordable Lithium Superionic Conductor. *J. Am. Chem. Soc.* **2013**, *135*, 15694−15697.

(4) Lin, Q.; Bu, X.; Mao, C.; Zhao, X.; Sasan, K.; Feng, P. Mimicking High-Silica Zeolites: Highly Stable Germanium- and Tin-Rich Zeolite-Type Chalcogenides. *J. Am. Chem. Soc.* **2015**, *137*, 6184−6187.

(5) Wang, K.-Y.; Feng, M.-L.; Kong, D.-N.; Liang, S.-J.; Wu, L.; Huang, X.-Y. Layered Indium Chalcogenidoantimonates $[Me_2NH_2]_2In_2Sb_2S_{7-x}Se_x$ (x = 0, 2.20, 4.20, 7) with Tunable Band Gaps and Photocatalytic Properties. *CrystEngComm* **2012**, *14*, 90−94.

(6) Yue, C.-Y.; Lei, X.-W.; Liu, R.-Q.; Zhang, H.-P.; Zhai, X.-R.; Li, W.-P.; Zhou, M.; Zhao, Z.-F.; Ma, Y.-X.; Yang, Y.-D. Syntheses, Crystal Structures, and Photocatalytic Properties of a Series of Mercury Thioantimonates Directed by Transition Metal Complexes. *Cryst. Growth Des.* **2014**, *14*, 2411−2421.

(7) Liu, Y.; Kanhere, P. D.; Ling Wong, C.; Tian, Y.; Feng, Y.; Boey, F.; Wu, T.; Chen, H.; White, T. J.; Chen, Z.; Zhang, Q. Hydrazine-Hydrothermal Method to Synthesize Three-Dimensional Chalcogenide Framework for Photocatalytic Hydrogen Generation. *J. Solid State Chem.* **2010**, *183*, 2644−2649.

(8) Kaga, H.; Saito, K.; Kudo, A. Solar Hydrogen Production over Novel Metal Sulfide Photocatalysts of $AGa_2In_3S_8$ (A = Cu or Ag) with Layered Structures. *Chem. Commun.* **2010**, *46*, 3779.
(9) Zhang, B.; Feng, M.-L.; Li, J.; Hu, Q.-Q.; Qi, X.-H.; Huang, X.-Y. Syntheses, Crystal Structures, and Optical and Photocatalytic Properties of Four Small-Amine-Molecule-Directed M−Sn−Q (M = Zn, Ag; Q = S, Se) Compounds. *Cryst. Growth Des.* **2017**, *17*, 1235−1244.
(10) Zhang, B.; Feng, M.-L.; Cui, H.-H.; Du, C.-F.; Qi, X.-H.; Shen, N.-N.; Huang, X.-Y. Syntheses, Crystal Structures, Ion-Exchange, and Photocatalytic Properties of Two Amine-Directed Ge−Sb−S Compounds. *Inorg. Chem.* **2015**, *54*, 8474−8481.
(11) Feng, M.-L.; Wang, K.-Y.; Huang, X.-Y. Combination of Metal Coordination Tetrahedra and Asymmetric Coordination Geometries of Sb(III) in the Organically Directed Chalcogenidometalates: Structural Diversity and Ion-Exchange Properties. *Chem. Rec.* **2016**, *16*, 582−600.
(12) Ding, N.; Kanatzidis, M. G. Selective Incarceration of Caesium Ions by Venus Flytrap Action of a Flexible Framework Sulfide. *Nat. Chem.* **2010**, *2*, 187−191.
(13) Manos, M. J.; Chrissafis, K.; Kanatzidis, M. G. Unique Pore Selectivity for Cs^+ and Exceptionally High NH_4^+ Exchange Capacity of the Chalcogenide Material $K_6Sn[Zn_4Sn_4S_{17}]$. *J. Am. Chem. Soc.* **2006**, *128*, 8875−8883.
(14) Manos, M. J.; Kanatzidis, M. G. Metal Sulfide Ion Exchangers: Superior Sorbents for the Capture of Toxic and Nuclear Waste-Related Metal Ions. *Chem. Sci.* **2016**, *7*, 4804−4824.
(15) Palchoudhury, S.; Ramasamy, K.; Han, J.; Chen, P.; Gupta, A. Transition Metal Chalcogenides for Next-Generation Energy Storage. *Nanoscale Adv.* **2023**, *5*, 2724−2742.
(16) Sajjad, M.; Cheng, F.; Lu, W. Research Progress in Transition Metal Chalcogenide Based Anodes for K-Ion Hybrid Capacitor Applications: A Mini-Review. *RSC Adv.* **2021**, *11*, 25450−25460.
(17) Cherusseri, J.; Choudhary, N.; Sambath Kumar, K.; Jung, Y.; Thomas, J. Recent Trends in Transition Metal Dichalcogenide Based Supercapacitor Electrodes. *Nanoscale Horiz.* **2019**, *4*, 840−858.
(18) Xia, H.; Xu, Q.; Zhang, J. Recent Progress on Two-Dimensional Nanoflake Ensembles for Energy Storage Applications. *Nano-Micro Lett.* **2018**, *10*, 66.
(19) Kaib, T.; Haddadpour, S.; Andersen, H. F.; Mayrhofer, L.; Järvi, T. T.; Moseler, M.; Möller, K.-C.; Dehnen, S. Quaternary Diamond-Like Chalcogenidometalate Networks as Efficient Anode Material in Lithium-Ion Batteries. *Adv. Funct. Mater.* **2013**, *23*, 5693−5699.
(20) Zhang, Q.; Chung, I.; Jang, J. I.; Ketterson, J. B.; Kanatzidis, M. G. Chalcogenide Chemistry in Ionic Liquids: Nonlinear Optical Wave-Mixing Properties of the Double-Cubane Compound $[Sb_7S_8Br_2](AlCl_4)_3$. *J. Am. Chem. Soc.* **2009**, *131*, 9896−9897.
(21) Morris, R. E. Ionothermal Synthesis—Ionic Liquids as Functional Solvents in the Preparation of Crystalline Materials. *Chem. Commun.* **2009**, 2990−2998.
(22) Lin, Z.; Wragg, D. S.; Warren, J. E.; Morris, R. E. Anion Control in the Ionothermal Synthesis of Coordination Polymers. *J. Am. Chem. Soc.* **2007**, *129*, 10334−10335.
(23) Wu, Z.; Weigend, F.; Fenske, D.; Naumann, T.; Gottfried, J. M.; Dehnen, S. Ion-Selective Assembly of Supertetrahedral Selenido Germanate Clusters for Alkali Metal Ion Capture and Separation. *J. Am. Chem. Soc.* **2023**, *145*, 3802−3811.
(24) Santner, S.; Yogendra, S.; Weigand, J. J.; Dehnen, S. Exploring the Chemical Reaction Space at the Formation of Chalcogenidometalate Superspheres in Ionic Liquids. *Chem. − Eur. J.* **2017**, *23*, 1999−2004.
(25) Santner, S.; Heine, J.; Dehnen, S. Synthesis of Crystalline Chalcogenides in Ionic Liquids. *Angew. Chem., Int. Ed.* **2016**, *55*, 876−893.
(26) Yu, J.-M.; Yu, J.-P.; Wang, N.; Xiao, L.-L.; Wang, H.; Xu, Q.; Zheng, B.; Cheng, F.-F.; Xiong, W.-W. Two Series of Main-Group Heterometallic Selenides Synthesized in Two Different Types of Ionic Liquids. *Inorg. Chem.* **2021**, *60*, 4337−4341.
(27) Lin, Y.; Massa, W.; Dehnen, S. "Zeoball" $[Sn_{36}Ge_{24}Se_{132}]^{24-}$: A Molecular Anion with Zeolite-Related Composition and Spherical Shape. *J. Am. Chem. Soc.* **2012**, *134*, 4497−4500.
(28) Wu, Z.; Tallu, M.; Stuhrmann, G.; Dehnen, S. Ligand-Functionalized and Ligand-Bridged or Organyl-Separated Chalcogenido Metalate-Based Clusters. *Coord. Chem. Rev.* **2023**, *497*, No. 215424.
(29) Wu, Z.; Stuhrmann, G.; Dehnen, S. Crystalline Chalcogenidometalate-Based Compounds from Uncommon Reaction Media. *Chem. Commun.* **2022**, *58*, 11609−11624.
(30) Shen, N.-N.; Hu, B.; Cheng, C.-C.; Zou, G.-D.; Hu, Q.-Q.; Du, C.-F.; Li, J.-R.; Huang, X.-Y. Discrete Supertetrahedral T3 InQ Clusters (Q = S, S/Se, Se, Se/Te): Ionothermal Syntheses and Tunable Optical and Photodegradation Properties. *Cryst. Growth Des.* **2018**, *18*, 962−968.
(31) Peters, B.; Stuhrmann, G.; Mack, F.; Weigend, F.; Dehnen, S. Highly Soluble Supertetrahedra upon Selective Partial Butylation of Chalcogenido Metalate Clusters in Ionic Liquids. *Angew. Chem., Int. Ed.* **2021**, *60*, 17622−17628.
(32) Du, C.-F.; Shen, N.-N.; Li, J.-R.; Hao, M.-T.; Wang, Z.; Huang, X.-Y. Synthesizing 2D and 3D Selenidostannates in Ionic Liquids: The Synergistic Structure-Directing Effects of Ionic Liquids and Metal-Amine Complexes. *Chem. − Asian J.* **2016**, *11*, 1555−1564.
(33) Peters, B.; Santner, S.; Donsbach, C.; Vöpel, P.; Smarsly, B.; Dehnen, S. Ionic Liquid Cations as Methylation Agent for Extremely Weak Chalcogenido Metalate Nucleophiles. *Chem. Sci.* **2019**, *10*, 5211−5217.
(34) Stuhrmann, G.; Schneider, J.; Schmidt, K.; Dehnen, S. Selective and Benign Alkylation of Sulfido-Oxo Stannate Clusters with Propyl, Pentyl, or Hexyl Substituents. *Chem. Commun.* **2023**, *59*, 13171−13174.
(35) Wu, Z.; Nußbruch, I.; Nier, S.; Dehnen, S. Ionothermal Access to Defined Oligomers of Supertetrahedral Selenido Germanate Clusters. *JACS Au* **2022**, *2*, 204−213.
(36) Biller, H.; Strassner, T. Synthesis and Physical Properties of Tunable Aryl Alkyl Ionic Liquids (TAAILs) Comprising Imidazolium Cations Blocked with Methyl-, Propyl- and Phenyl-Groups at the C2 Position. *Chem. − Eur. J.* **2023**, *29*, No. e202202795.
(37) Lerch, S.; Fritsch, S.; Strassner, T. The Mizoroki-Heck Reaction in Tunable Aryl Alkyl Ionic Liquids. *Eur. J. Org. Chem.* **2022**, *2022*, No. e202200008.
(38) Lerch, S.; Strassner, T. Synthesis and Physical Properties of Tunable Aryl Alkyl Ionic Liquids (TAAILs). *Chem. − Eur. J.* **2021**, *27*, 15554−15557.
(39) Lerch, S.; Strassner, T. Expanding the Electrochemical Window: New Tunable Aryl Alkyl Ionic Liquids (TAAILs) with Dicyanamide Anions. *Chem. − Eur. J.* **2019**, *25*, 16251−16256.
(40) Zaitsau, D. H.; Kaliner, M.; Lerch, S.; Strassner, T.; Emel'yanenko, V. N.; Verevkin, S. P. Thermochemical Properties of Tunable Aryl Alkyl Ionic Liquids (TAAILs) Based on Phenyl-1 *H* -Imidazoles: Thermochemical Properties of Tunable Aryl Alkyl Ionic Liquids (TAAILs) Based on Phenyl-1 *H* -Imidazoles. *Z. Anorg. Allg. Chem.* **2017**, *643*, 114−119.
(41) Ahrens, S.; Peritz, A.; Strassner, T. Tunable Aryl Alkyl Ionic Liquids (TAAILs): The Next Generation of Ionic Liquids. *Angew. Chem., Int. Ed.* **2009**, *48*, 7908−7910.
(42) Lerch, S.; Fritsch, S.; Strassner, T. Friedel−Crafts Acylation of Benzene Derivatives in Tunable Aryl Alkyl Ionic Liquids (TAAILs). *Beilstein J. Org. Chem.* **2023**, *19*, 212−216.
(43) Schroeter, F.; Lerch, S.; Kaliner, M.; Strassner, T. Cobalt-Catalyzed Hydroarylations and Hydroaminations of Alkenes in Tunable Aryl Alkyl Ionic Liquids. *Org. Lett.* **2018**, *20*, 6215−6219.
(44) Schmolke, L.; Lerch, S.; Bülow, M.; Siebels, M.; Schmitz, A.; Thomas, J.; Dehm, G.; Held, C.; Strassner, T.; Janiak, C. Aggregation Control of Ru and Ir Nanoparticles by Tunable Aryl Alkyl Imidazolium Ionic Liquids. *Nanoscale* **2019**, *11*, 4073−4082.
(45) Woitassek, D.; Strothmann, T.; Biller, H.; Lerch, S.; Schmitz, H.; Song, Y.; Roitsch, S.; Strassner, T.; Janiak, C. Tunable Aryl Alkyl Ionic Liquid Supported Synthesis of Platinum Nanoparticles and

https://doi.org/10.1021/acs.inorgchem.5c05009
Inorg. Chem. XXXX, XXX, XXX−XXX

Their Catalytic Activity in the Hydrogen Evolution Reaction and in Hydrosilylation. *Molecules* **2023**, *28*, 405.
(46) Woitassek, D.; Lerch, S.; Jiang, W.; Shviro, M.; Roitsch, S.; Strassner, T.; Janiak, C. The Facile Deposition of Pt Nanoparticles on Reduced Graphite Oxide in Tunable Aryl Alkyl Ionic Liquids for ORR Catalysts. *Molecules* **2022**, *27*, 1018.
(47) Wachhold, M.; Kanatzidis, M. G. Surfactant-Templated Inorganic Lamellar and Non-Lamellar Hybrid Phases Containing Adamantane $[Ge_4Se_{10}]^{4-}$ Anions. *Chem. Mater.* **2000**, *12*, 2914−2923.
(48) Pohl, S.; Krebs, B. Darstellung und Struktur von $Cs_4Ge_4S_{10}\cdot 3H_2O$. *Z. Anorg. Allg. Chem.* **1976**, *424*, 265−272.
(49) Brandsma, L.; Wijers, H. E. A Simple Laboratory Scale Preparative Method for Dialkyl Sulphides, Selenides, Tellurides, Thiols and Selenols. *Recl. Trav. Chim. Pays-Bas* **1963**, *82*, 68−74.
(50) Murphy, A. Band-Gap Determination from Diffuse Reflectance Measurements of Semiconductor Films, and Application to Photoelectrochemical Water-Splitting. *Sol. Energy Mater. Sol. Cells* **2007**, *91*, 1326−1337.
(51) Kubelka, P.; Munk, F. Ein Beitrag Zur Optik Der Farbanstriche. *Z. Techn. Phys.* **1931**, *12*, 593−601.
(52) Tauc, J.; Grigorovici, R.; Vancu, A. Optical Properties and Electronic Structure of Amorphous Germanium. *Phys. Status Solidi B* **1966**, *15*, 627−637.
(53) Makuła, P.; Pacia, M.; Macyk, W. How To Correctly Determine the Band Gap Energy of Modified Semiconductor Photocatalysts Based on UV−Vis Spectra. *J. Phys. Chem. Lett.* **2018**, *9*, 6814−6817.
(54) Michalow, K. A.; Logvinovich, D.; Weidenkaff, A.; Amberg, M.; Fortunato, G.; Heel, A.; Graule, T.; Rekas, M. Synthesis, Characterization and Electronic Structure of Nitrogen-Doped TiO_2 Nanopowder. *Catal. Today* **2009**, *144*, 7−12.
(55) Loose, A.; Sheldrick, W. S. Synthesis and Structure of $[Sn_4Se_{11}]^{6-}$, $^{\infty}_1[Sn_2Se_5^{2-}]$, and $^{\infty}_1[Sn_3Se_7^{2-}]$ - Model Anions for the Solventothermal Reaction Pathway to Lamellar Selenidostannates(IV). *Z. Anorg. Allg. Chem.* **1999**, *625*, 233−240.
(56) Peters, B.; Lichtenberger, N.; Dornsiepen, E.; Dehnen, S. Current Advances in Tin Cluster Chemistry. *Chem. Sci.* **2020**, *11*, 16−26.
(57) Tang, S.; Liu, X.; Zhou, J. A Series of Dimeric Selenidogermanates with Lanthanide Complexes of Multidentate Chelating Amines. *J. Clust. Sci.* **2017**, *28*, 2589−2600.
(58) Luo, M.; Hu, D.; Yang, H.; Li, D.; Wu, T. PCU-Type Copper-Rich Open-Framework Chalcogenides: Pushing up the Length Limit of the Connection Mode and the First Mixed-Metal $[Cu_7GeSe_{13}]$ Cluster. *Inorg. Chem. Front.* **2017**, *4*, 387−392.
(59) Luo, H.-Y.; Zhou, J. A Series of New Hybrid Selenidostannates with Metal Complexes Prepared in Alkylol Amines. *Dalton Trans.* **2018**, *47*, 14751−14759.
(60) Han, X.; Meng, J.; Xu, J.; Liu, X.; Liu, D.; Wang, C. Synthesis, Crystal Structure, and Optical Property of a One-Dimensional Selenidostannate: $[AEPPH_2]_2[Sn_5Se_{12}]$ (AEPP = N -Aminoethylpiperazine). *Inorg. Chem. Commun.* **2016**, *63*, 42−47.
(61) Lin, Y.; Massa, W.; Dehnen, S. Controlling the Assembly of Chalcogenide Anions in Ionic Liquids: From Binary Ge/Se through Ternary Ge/Sn/Se to Binary Sn/Se Frameworks. *Chem. − Eur. J.* **2012**, *18*, 13427−13434.
(62) Santner, S.; Wolff, A.; Ruck, M.; Dehnen, S. Multi-Valent Group 14 Chalcogenide Architectures from Ionic Liquids: 0D-$\{[Cs@Sn^{II}_4(Ge^{IV}_4Se_{10})_4]^{7-}\}$ and 2D-$\{[Sn^{II}(Ge^{IV}_4Se_{10})]^{2-}\}$. *Chem. − Eur. J.* **2018**, *24*, 11899−11903.
(63) Ahari, H.; Lough, A.; Petrov, S.; Ozin, G. A.; Bedard, R. L. Modular Assembly and Phase Study of Two- and Three-Dimensional Porous Tin(IV) Selenides. *J. Mater. Chem.* **1999**, *9*, 1263−1274.
(64) Lu, S.; Ke, Y.; Li, J.; Zhou, S.; Wu, X.; Du, W. Solvothermal Synthesis and Structure of Two 2D Tin−Selenides with Long Alkyldiamine $NH_2(CH_2)_nNH_2$ (n = 8, 10). *Struct. Chem.* **2003**, *14*, 637−642.
(65) Li, J.-R.; Xiong, W.-W.; Xie, Z.-L.; Du, C.-F.; Zou, G.-D.; Huang, X.-Y. From Selenidostannates to Silver-Selenidostannate: Structural Variation of Chalcogenidometallates Synthesized in Ionic Liquids. *Chem. Commun.* **2013**, *49*, 181−183.
(66) Xiong, W.; Miao, J.; Ye, K.; Wang, Y.; Liu, B.; Zhang, Q. Threading Chalcogenide Layers with Polymer Chains. *Angew. Chem., Int. Ed.* **2015**, *54*, 546−550.
(67) Tallu, M.; Peters, B.; Friedrich, A.; Dehnen, S. Ionothermal Approach to Homo- and Heteroleptic Alkylation of Tellurido Mercurate Clusters for Assembly in Lamellar Crystal Structures. *Inorg. Chem.* **2023**, *62*, 13943−13952.
(68) Donsbach, C.; Reiter, K.; Sundholm, D.; Weigend, F.; Dehnen, S. $[Hg_4Te_8(Te_2)_4]^{8-}$: A Heavy Metal Porphyrinoid Embedded in a Lamellar Structure. *Angew. Chem., Int. Ed.* **2018**, *57*, 8770−8774.
(69) Rangan, K. K.; Kanatzidis, M. G. Mesolamellar Thiogermanates $[C_nH_{2n+1}NH_3]_4Ge_4S_{10}$. *Inorg. Chim. Acta* **2004**, *357*, 4036−4044.

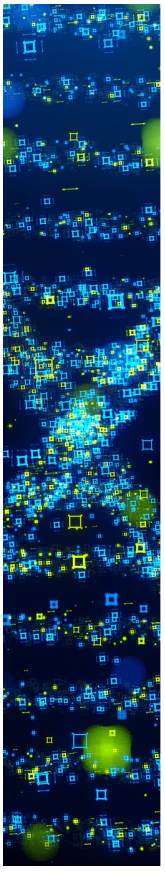

https://doi.org/10.1021/acs.inorgchem.5c05009
Inorg. Chem. XXXX, XXX, XXX−XXX